Molecular dynamics of topological and chemical orders in liquid $Al_{1-x}Mn_x$ alloys

1994 J. Phys.: Condens. Matter 6 2853

(http://iopscience.iop.org/0953-8984/6/15/008)

J. Phys.: Condens. Matter 6 (1994) 2853–2860. Printed in the UK

Molecular dynamics of topological and chemical orders in liquid $Al_{1-x}Mn_x$ alloys

L Do Phuong, D Nguyen Manh† and A Pasturel

Laboratoire de Thermodynamique et de Physico-Chimie Métallurgiques, Ecole Nationale Supérieure d'Electrochimie et d'Electrométallurgie de Grenoble, BP 75, 38402 St-Martin-d'Hères Cédex, France

Received 25 November 1993

Abstract. We present an atomistic simulation of the structure of liquid $Al_{1-x}Mn_x$ alloys based on interatomic forces derived from quantum theory. Using the intra-atomic potentials calculated within the tight-binding bond approach, we study the structural properties of liquid $Al_{80}Mn_{20}$ and $Al_{60}Mn_{40}$ alloys using molecular dynamics simulations. The results are in good agreement with the most accurate diffraction data. The correlation of the structural trend with the characteristic variation in the electronic structure is established.

1. Introduction

The atomic structure of liquid aluminium–transition-metal alloys has been the subject of intense research over the last 3 years [1–3]. These results, based on neutron diffraction measurements have given us clues that indicate icosahedral order in the number–number structure factor $S_{NN}(q)$ of liquid $Al_{1-x}Mn_x$ alloys, which are absent for liquid $Al_{80}Ni_{20}$; these are the existence of a sharp first peak, a height ratio of the two first peaks close to the value obtained from a Landau description of short-range icosahedral order [4], and a shape of the second peak that tends to form a double-component peak at positions $1.7q_1$ and $2q_1$. However, for liquid materials, diffraction studies lead to a set of partial pair correlation functions, i.e. to a one-dimensional projection of a three-dimensional structure. Hence a fundamental understanding of the liquid structure is possible only if the diffraction experiments can be supplemented by accurate modelling structures. However, an accurate simulation of the properties of transition metals and of their alloys is still a challenging problem since bonding is not well described by the currently available pair and embedded-atom potentials. Very recently, a bond-order approach to interatomic interactions has been proposed [5, 6]. This bond-order approach is derived from tight-binding Hückel theory in which the quantum-mechanical bond energy in a given pair of atoms i and j is written in the chemically intuitive form

$$U_{\text{bond}}(i, j) = \sum_{\alpha,\beta} \Phi^{\text{bond}}_{\alpha(i),\beta(j)} = 2 \sum_{\alpha,\beta} H_{i\alpha,j\beta}\Theta_{i\alpha,j\beta} \tag{1}$$

where $H_{i\alpha,j\beta}$ is the Slater–Koster bond integral matrix linking the orbitals α, β on site i and j together. Θ is the corresponding bond-order matrix whose elements give the difference between the number of electrons in the bonding $(1/\sqrt{2})|i\alpha + j\beta\rangle$ and antibonding states

† Permanent address: Department of Physics, Polytechnic University of Hanoi, Vietnam.

0953-8984/94/152853+08$19.50

$(1/\sqrt{2})|i\alpha - j\beta\rangle$. Bond-order potentials are similar to the embedding potentials in that the bond in a given pair of atoms is considered as embedded in and depending on the local atomic environment. Thus, equation (1) represents only formally a pair interaction and depends via the bond order on many-atom effects. The explicit analytical form of these many-body potentials has the necessary ingredient for an adequate description, but there are difficulties in practice when it comes to incorporating the charge-transfer contribution between different orbitals in a self-consistent way. The last remark has encouraged us to develop a new simple effective pair interaction for pure liquid transition metals and transition-metal-based alloys [7, 8]. The bond order is calculated from the tight-binding scalar Bethe lattice method (SCBLM) which is expected to be valid in disordered systems. Indeed, for a disordered system, the detailed structure in the electronic density of states (DOS) which is the origin of the characteristic variations in the higher moments and hence in the many-body interactions is smeared out. Therefore, it is possible to use approximation such as the cluster Bethe lattice method (CBLM) which gives the correct fourth moment of the local DOS and then reproduces the band-mixing effect correctly. In this paper, our approach is applied to liquid aluminium–manganese alloys. It turns out that the bond orders depend very sensitively on the partial DOSs in the alloy which are calculated for each composition self-consistently. As the electronic DOS of Al–Mn alloys is characterized by strong hybridization between the sp orbitals of Al and the d orbitals of Mn, the pair forces in the alloy are essentially concentration dependent and the non-additive potentials have a strong preference for the formation of pairs of unlike atoms and short-bond distances in the Al–Mn pairs. In the liquid structures, this is reflected in a composition dependence of topological and chemical short-range order. We note that our approach is the first to reproduce a quantum-mechanical force field for liquid Al–Mn alloys which can be used in atomistic simulations.

2. Tight-binding approach to interatomic forces

Within the tight-binding bond (TBB) approximation, the binding energy may be written in the form [5, 6]

$$U_{\text{bind}} = \tfrac{1}{2}\sum_i \sum_{j(\neq i)} [\Phi^{\text{rep}}(r_{ij}) + U_{\text{bond}}(i, j)]. \tag{2}$$

Equation (2) is derived with the assumption that each atom is assumed to remain charge neutral by varying the on-site Hamiltonian matrix elements in such a way that the energy splittings between different orbitals on the same atom are preserved [9]. This approximation ensures that the TBB model is consistent with the force theorem.

The bond-order matrix entering the definition of the bonding energy (see equation (1)) can be expressed as

$$\Theta_{i\alpha,j\beta} = -\frac{2}{\pi}\int^{E_F} \text{Im}[G_{ij}^{\alpha\beta}(E)]\,\text{d}E. \tag{3}$$

In order to calculate the Green function $G_{ij}^{\alpha\beta}(E)$, we have used the SCBLM for which the mean local environment is isotropic and there is a spherical point symmetry for the CBLM mean-field model [10]. In order to obtain the bond order in the SCBLM formalism, we first recall the matrix expression for the Green function of an atom in the CBLM [10]:

$$G_I^{\text{CBLM}}(z) = \left(z1 - E_I - Z\sum_J p_{IJ}t_{IJ}S_{IJ}(z)\right)^{-1} \tag{4}$$

where $I(i)$ denotes the species A or B at site i, p_{IJ} are the pair probabilities, and $\mathbf{t}_{IJ}$ and $\mathbf{S}_{IJ}$ are the matrix of hopping energies and the so-called transfer matrix, respectively. In the spherical approximation made by the SCBLM, we obtain simple scalar equations for the Green function in the subspaces $\alpha(i)$ of atom i as [7]

$$G_{\alpha(i)}(z) = \left(z - E_{\alpha(i)} - Z\sum_{\beta(j)} \sigma^2_{\alpha(i),\beta(j)} G'_{\beta(j)}(z)\right)^{-1} \tag{5}$$

where one defines

$$\sigma^2_{\alpha(i),\beta(j)} = Z p_{IJ} n_\beta T^2_{\alpha(i),\beta(j)} \tag{6}$$

where n_β is the degeneracy of the subspace β and $T^2_{\alpha(i),\beta(j)}$ is the mean square of the matrix element between a state of subspace α of atom i and a state of subspace β of atom j (see equation (10) in [10]). Finally, $G'_{\beta(j)}(z)$ can be defined by

$$G'_{\beta(j)} = \left(z - E_{\beta(j)} - \sum_{\gamma(k)} \sigma'^2_{\beta(j),\gamma(k)} G_{\gamma(k)}(z)\right)^{-1} \tag{7}$$

with $\sigma'^2_{\beta(j),\gamma(k)} = [(Z-1)/Z]\sigma^2_{\beta(j),\gamma(k)}$. By comparing (4) with (5) and (6) it follows that

$$t_{\alpha(i)\beta(j)} S_{\beta(j)\alpha(i)}(z) = n_\beta T^2_{\alpha(i)\beta(j)} G'_{\beta(j)}(z). \tag{8}$$

On the other hand, the transfer matrix $\mathbf{S}$ is related to the off-diagonal Green function by

$$G_{\beta(j)\alpha(i)}(z) = \sum_\alpha S_{\beta(j)\alpha(i)} G_{\alpha(i)\alpha(i)}(z) = n_\alpha S_{\beta(j)\alpha(i)} G_{\alpha(i)}(z). \tag{9}$$

Then, the bond potential can be written as

$$U^{ij}_{\text{bond}} = -\frac{2}{\pi}\sum_{\alpha\beta} t_{\alpha(i)\beta(j)} \operatorname{Im}\left(\int^{E_F} n_\alpha S_{\beta(j)\alpha(i)}(E) G_{\alpha(i)}(E)\,\mathrm{d}E\right) \tag{10}$$

$$= -\frac{2}{\pi}\sum_{\alpha\beta} \operatorname{Im}\left(\int^{E_F} n_\alpha n_\beta T^2_{\alpha(i)\beta(j)} G_{\alpha(i)}(E) G'_{\beta(j)}(E)\,\mathrm{d}E\right) = \sum_{\alpha\beta} \Phi^{\text{bond}}_{\alpha(i)\beta(j)}.$$

From equation (10) it is clear that the bond–potential interaction can be expressed directly from the local Green functions treated in the mean isotropic environment. The advantage of equation (10) is that it allows us to estimate the different orbital contributions in the bond energy and more particularly to treat the effect of hybridization explicitly.

Assuming that the distance dependence of the bond order $\Theta_{j\beta,i\alpha}$ in equation (3) is negligible with respect to that of the transfer integral [5] we obtain

$$\Phi^{\text{bond}}_{\alpha(i)\beta(j)} = t_{\alpha(i)\beta(j)} \Theta_{j\beta,i\alpha} \tag{11}$$

with the distance dependence of the hopping integral $t_{\alpha(i)\beta(j)}$. Here the average hopping integrals are evaluated according to Harrison's [11] power-law dependence:

$$(ll'm) = \eta_{ll'm}(h^2/mr^2) \tag{12}$$

for s, p electrons and

$$(ll'm) = \eta_{ll'm}(h^2/mr^{l+l'+1}) \tag{13}$$

for other electrons. To determine the repulsive part of the binding energy, we assume repulsive pairwise interactions as expressed in equation (2), with given $\Phi_{IJ}^{\mathrm{rep}}(r_{ij})$ given by

$$\Phi_{IJ}^{\mathrm{rep}}(r_{ij}) = \sum_{\alpha,\beta} \Phi_{\alpha(I)\beta(J)}^{\mathrm{rep}}(r_{ij}) = \frac{1}{2}\sum_{\alpha,\beta}\left(\frac{C_{\alpha(I)}C_{\beta(J)}}{r_{ij}^{m_\alpha+m_\beta}}\right)^{1/2}. \tag{14}$$

For s–s and p–p interactions, the repulsive pair interaction is modelled as $\Phi_{\alpha\alpha}^{\mathrm{rep}}(r_{ij}) = c_{\alpha\alpha}/r_{ij}^4$, while for d–d interactions a stronger power-law dependence $c_{\mathrm{dd}}/r_{ij}^{10}$ is chosen. $C_{\alpha\alpha}$ ($\alpha \equiv$ s, p or d orbitals) are the only parameters of the model; they are determined from knowledge of the experimental atomic volume and bulk modulus of the pure metals. To treat the alloying effect, i.e. the Al–Mn interactions, we have to determine the attractive and the repulsive parts of the heteroatomic bond potential. The parametrization of the repulsive pair interaction is still achieved using equation (14) with the same $C_{\alpha(\mathrm{A})}$- and $C_{\beta(\mathrm{B})}$-values. To obtain the $h_{\mathrm{A}\alpha,\mathrm{B}\beta}$ hopping integrals (i.e. $(\mathrm{ss}\sigma)_{\mathrm{AB}}$, $(\mathrm{sp}\sigma)_{\mathrm{AB}}$, $(\mathrm{sd}\sigma)_{\mathrm{AB}}$, $(\mathrm{pd}\sigma)_{\mathrm{AB}}$ and $(\mathrm{pd}\pi)_{\mathrm{AB}}$), we use the geometrical average of hopping integrals given in table 1, which is reasonable in the case of the alloys studied. Consequently, no parameters are introduced to describe the alloy properties. At the end, the dependence for both hopping integral and repulsive terms has been modified using the rescaling method proposed by Goodwin *et al* [12]. This method is known for generating improved tight-binding parameters which are both transferable and suitable for extensive molecular dynamics simulations. The two scaling parameters of the scaling smoothed step function, namely r_c and n_c, have been chosen in such a way that the step is positioned between the first- and the second-nearest neighbours in the FCC lattice and that the interactions become zero at $\frac{1}{2}L$, where L is the linear dimension of the molecular dynamic cell. Table 1 shows all the parameters entering the interatomic interactions.

Table 1. Tight-binding and repulsive parameters for Al, Mn and Ni.

	TB parameters (eV)								Repulsive parameters (eV)		
	sss	dds	ddp	ddd	sds	pps	ppp	sps	C_{ss}	C_{dd}	C_{pp}
Al	−0.52					1.20	−0.31	0.71	0.30		0.30
Mn	−1.33	−0.65	0.32	0.00	−1.15				1.22	0.07	

3. Structure of liquid $Al_{80}Mn_{20}$ and $Al_{60}Mn_{40}$ alloys

During the last few years, we have focused attention on the study of topological and chemical short-range order in aluminium–transition-metal liquid alloys [1–3] through the accurate determination of the partial pair correlation functions by neutron diffraction. In the experimental study of composition dependence of topological and chemical short-range order in liquid $Al_{1-x}Mn_x$ alloys, the most salient features are the following: the comparison between $Al_{80}Mn_{20}$ and $Al_{60}Mn_{40}$ liquids has shown that the strength of the heteroatomic interactions is similar in both alloys and that, by contrast, the local arrangements between homoatomic pairs change significantly with Mn concentration, as indicated by the shortening of the Mn–Mn and Al–Al first-neighbour distances in $Al_{60}Mn_{40}$. Then it is important to know whether our interactions are able to reproduce such differences. Therefore the molecular dynamic simulations of liquid $Al_{80}Mn_{20}$ and $Al_{60}Mn_{40}$ alloys were performed at constant volume and constant temperature [7, 8]. We consider a system of 1332 atoms in a

cubic box with periodic boundary conditions such that the composition and the density of the two systems are equal to the experimental values. The initial atomic positions are randomly chosen. The Newtonian equations of motion were solved using the Verlet algorithm with a time increment of 310^{-15} s. Classical dynamical trajectories of 10^4 time steps were generated to calculate properties of the alloy.

The reduced partial pair distribution functions $G_{ij}(r)$ of the liquid $Al_{80}Mn_{20}$ and $Al_{60}Mn_{40}$ alloys shown in figure 1 are the curves averaged over the last 100 000 integration steps. They are in phase with the experimental curves and, more particularly, reproduce the experimental height and position of the peaks. By comparing the two curves, we can see that the Mn–Al distributions are exactly in phase, indicating that the strength of heteroatomic interactions associated with the sp–d hybridization is independent of the liquid-alloy composition. By contrast, the Mn–Mn first-pair distributions are different, since for $Al_{60}Mn_{40}$ the first peak of $G_{MnMn}(r)$ is shifted to smaller r-values. The comparison of Al–Al distributions shows a small shortening of the first distances. In table 2, the first interatomic distances (taken from the peak positions of the partial pair correlation functions $g_{ij}(r) = G_{ij}(r)/4\pi\rho r + 1$) are reported for both alloys with the corresponding partial coordination numbers calculated as follows:

$$z_{ij} = c_j \int_{r_{ij,\min}}^{r_{ij,\max}} \varphi_{\mathrm{RDF}_{ij}}(r)\,\mathrm{d}r \tag{15}$$

with $\varphi_{\mathrm{RDF}_{ij}}(r) = rG_{ij}(r) + 4\pi r^2\rho$. In equation (14), $r_{ij,\min}$ and $r_{ij,\max}$ are the lower and upper limits of the first coordination shell given by the minima in $G_{NN}(r)$. The agreement with experimental data is good and the most salient feature is that the nearest-neighbour distances for the three types of pairs are closer to each other in $Al_{60}Mn_{40}$ than in $Al_{80}Mn_{20}$. As mentioned above, it is essentially due to the shortening of the first Mn–Mn interatomic distance in $Al_{60}Mn_{40}$ which become shorter than Al–Al distances. For $Al_{60}Mn_{40}$ alloy, the Mn–Mn interatomic distance is 2.58 Å while the Mn–Al and Al–Al interatomic distances are 2.52 Å and 2.72 Å, respectively. In $Al_{80}Mn_{20}$ alloy, they have been found to be equal to 2.86 Å, 2.57 Å and 2.79 Å, respectively. The first Mn–Mn distance in $Al_{60}Mn_{40}$ becomes comparable with the value of pure liquid Mn (2.68 Å, [13]) and we think that Mn atoms have a peculiar behaviour in $Al_{80}Mn_{20}$ alloy. On the other hand, the Mn–Al distances are similar in $Al_{80}Mn_{20}$ and $Al_{60}Mn_{40}$ alloys and we conclude that the strength of chemical interactions is comparable in both alloys. This is confirmed by the calculation of the Warren chemical short-range order parameter generalized by Wagner and Ruppersberg [14] which is equal to -0.09 for $Al_{60}Mn_{40}$ and -0.04 for $Al_{80}Mn_{20}$, very close to the experimental values which are -0.07 and -0.06, respectively.

Table 2. Interatomic distances and coordination numbers in the liquid $Al_{80}Mn_{20}$ and $Al_{60}Mn_{40}$ alloys: comparison with experimental data [1,3].

	Liquid $Al_{80}Mn_{20}$		Liquid $Al_{60}Mn_{40}$	
Atomic pair	r_{ij} (Å)	z_{ij}	r_{ij} (Å)	z_{ij}
Mn–Mn	2.86 (2.89)	(1.5)	2.58 (2.61)	(4.5)
Mn–Al	2.57 (2.56)	(9.5)	2.52 (2.59)	(7.8)
Al–Al	2.79 (2.74)	(10.2)	2.72 (2.65)	(7.4)

The first conclusions obtained from the comparison between the $Al_{80}Mn_{20}$ and $Al_{60}Mn_{40}$ liquids are the following.

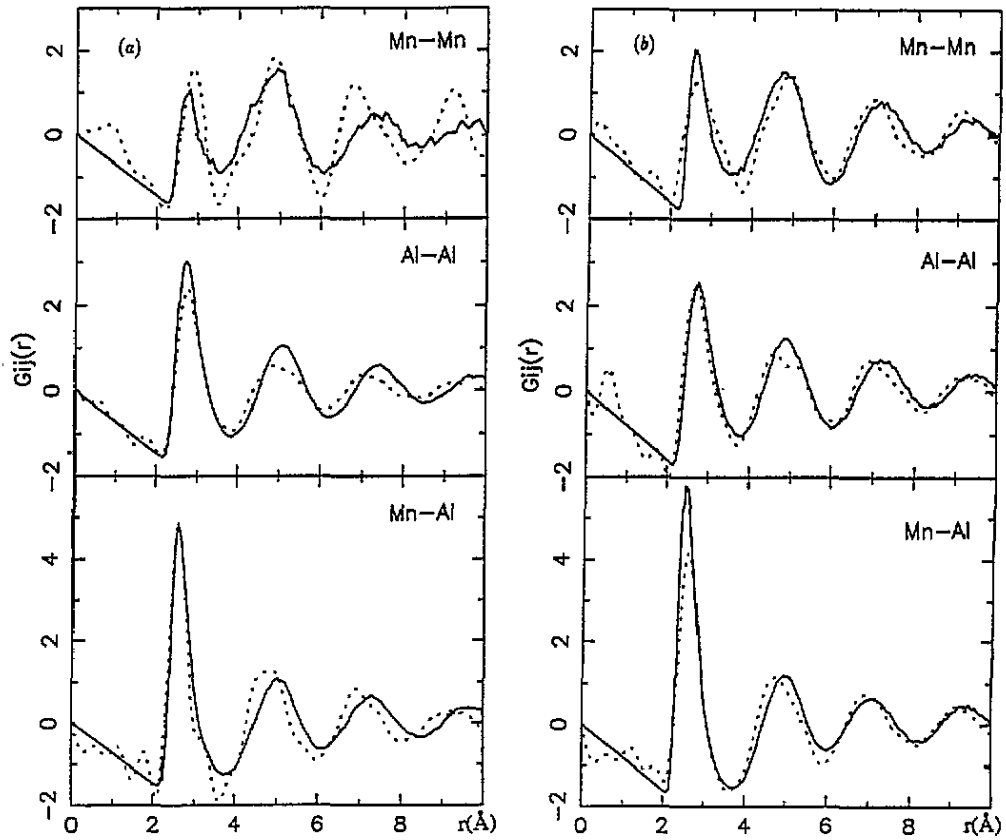

Figure 1. Reduced partial pair distribution functions $G_{ij}(r)$ for (*a*) $Al_{80}Mn_{20}$ and (*b*) $Al_{60}Mn_{40}$: ——, calculation; · · · · · ·, experiments [1,3].

(i) The chemical short-range order is similar in both alloys because the heteroatomic interactions display the same strength.

(ii) The topological short-range orders are different, as the homoatomic pairs change significantly with the transition-metal content, as indicated by the shortening of first Mn–Mn distances in $Al_{60}Mn_{40}$.

The fact that the topological short-range orders are different in the two alloys is also confirmed by the bond-angle distribution functions (figure 2). For $Al_{80}Mn_{20}$, the calculated distribution shows a prominent peak near 63° and a broad maximum near 115°, very close to the icosahedral bond angles θ of 63.5° and 116.5°. For $Al_{60}Mn_{40}$, the distribution is shifted towards smaller bond-angle values and the peak near 60° is less prominent than in $Al_{80}Mn_{20}$.

These changes may now be traced back to the variations in the interatomic forces and in the electronic structure. As shown in figure 3 for both alloys, the strong pd hybridization leads to a strong interaction between Al and Mn atoms for both liquids; the consequence is the formation of pairs of unlike atoms and short-bond distances in the Al–Mn pairs. However, an important difference is in the evolution of the homoatomic interactions as a function of the composition. The $Al_{80}Mn_{20}$ alloy is characterized by a weak Mn–Mn

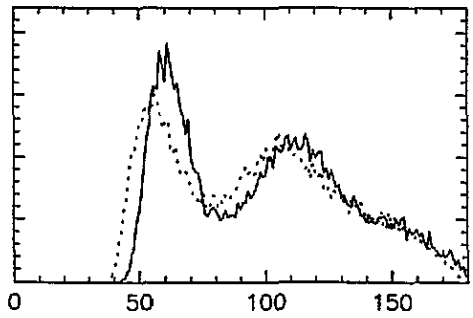

Figure 2. Calculated bond-angle distributions: ——, liquid $Al_{80}Mn_{20}$; ·····, liquid $Al_{60}Mn_{40}$.

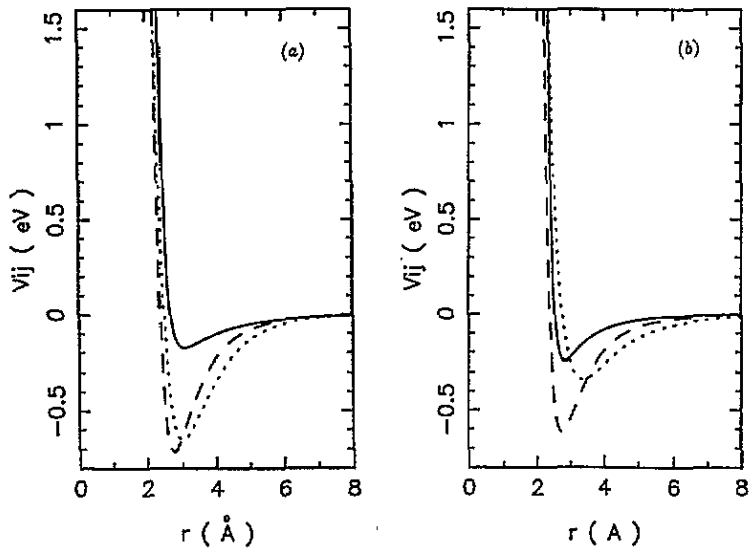

Figure 3. TBB potentials (eV) for (*a*) $Al_{80}Mn_{20}$ and (*b*) $Al_{60}Mn_{40}$: ——, Mn–Mn interaction; - - - -, Mn–Al interaction; ·····, Al–Al interaction.

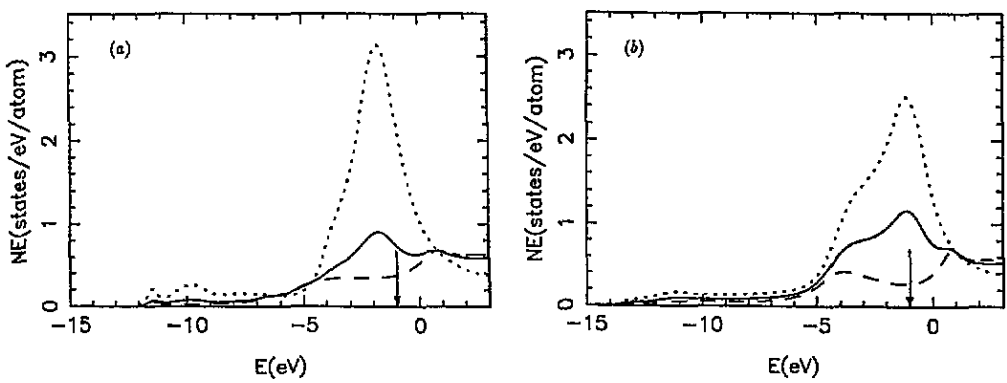

Figure 4. Calculated DOS for the liquid alloys (*a*) $Al_{80}Mn_{20}$ and (*b*) $Al_{60}Mn_{40}$: ——, total DOS; ·····, Mn partial DOS; - - - -, Al partial DOS.

interaction but a strong Al–Al interaction. As the Mn content increases, i.e. $Al_{60}Mn_{40}$ alloy, the strength of the Al–Al interaction decreases to become similar to Mn–Mn interactions but shifted to higher r-values. The electronic DOSs of both alloys are displayed in figure 4. They are obtained from the atomic coordinates obtained by molecular dynamics simulations

and the same tight-binding Hamiltonian but now coupled with the recursion method. The shape of both DOSs is characterized by a Mn d band coupled with a broad Al sp band. The major difference is in the shape of the d band and the location of the Fermi level. This is because Mn–Mn distances are shorter in $Al_{60}Mn_{40}$ alloy and the corresponding first-neighbour number is much larger than in $Al_{80}Mn_{20}$ alloy. The consequence is that Mn atoms in $Al_{60}Mn_{40}$ alloy retain a behaviour similar to pure Mn liquid. For $Al_{80}Mn_{20}$ alloy, the Fermi level is not located in the middle of the d band as for pure Mn [7] or for $Al_{60}Mn_{40}$ alloy. The overall shape of liquid alloy is very similar to that of α-(Al–Mn) as calculated by Fujiwara [15]. The major feature of the calculated DOS of α-(Al–Mn) is a dip or quasi-gap in the vicinity of the Fermi level; the quasi-gap was attributed to an antiresonance, with the resonance below the Fermi level. In the hypothetical binary Al–Mn case, the Fermi level resides at the lower-energy end of the quasi-gap. However, the origin of the DOS structure in the liquid $Al_{80}Mn_{20}$ alloy is quite different since the interatomic distances and coordination numbers in the first and second shells are different for the liquid and α-phases [1]. Let us recall that the Mn–Mn distance is longer in the liquid phase while, by contrast, the first Al–Al distance is shorter and the corresponding first-neighbour number is slightly larger. We think that in the liquid case a strong Al p–Mn d hybridization but also an important Al p–Al p coupling due to the short Al–Al bond length are at the origin of the $Al_{80}Mn_{20}$ DOS structures.

4. Conclusion

We have studied the structural and electronic properties of $Al_{80}Mn_{20}$ and $Al_{60}Mn_{40}$ liquid alloys using atomistic simulations based on TBB interatomic interactions. We have shown that the topological short-range orders in the two alloys differ significantly, in agreement with experimental results. Our results indicate icosahedral order in liquid $Al_{80}Mn_{20}$ which is absent for liquid $Al_{60}Mn_{40}$. We think that it is mainly due to the peculiar behaviour of Mn–Mn interactions in $Al_{80}Mn_{20}$ alloy.

References

[1] Maret M, Pasturel A, Senillou C, Dubois J M and Chieux P 1989 *J. Physique* **50** 295
[2] Maret M, Pomme T, Pasturel A and Chieux P 1990 *Phys. Rev.* B **42** 1598
[3] Maret M, Chieux P, Dubois J M and Pasturel A 1991 *J. Phys.: Condens. Matter* **3** 2801
[4] Sachdev S and Nelson D R 1985 *Phys. Rev.* B **32** 4592
[5] Pettifor D G 1989 *Phys. Rev. Lett.* **63** 2480
[6] Pettifor D G 1990 *Many-Atom Interactions in Solids* ed R M Nieminen, M J Puska and M J Manninen (Berlin: Springer) p 64
[7] Do Phuong L, Nguyen Manh D and Pasturel A 1993 *J. Phys.: Condens. Matter* **5** 1901
[8] Do Phuong L, Nguyen Manh D and Pasturel A 1993 *Phys. Rev. Lett.* **71** 372
[9] Sutton A P, Finnis M W, Pettifor D G and Ohta Y 1988 *J. Phys. C: Solid State Phys.* **21** 35
[10] Mayou D, Nguyen Manh D, Pasturel A and Cyrot Lackmann F 1986 *Phys. Rev.* B **33** 3384
[11] Harrison W A 1980 *Electronic Structure and the Properties of Solids* (San Francisco, CA: Freeman)
[12] Goodwin L, Skinner A J and Pettifor D G 1989 *Europhys. Lett.* **9** 701
[13] Waseda Y 1977 *Liquid Metals 1976 (Inst. Phys. Conf. Ser. 30)* ed R Evans and D Greenwood (Bristol: Institute of Physics) p 230; 1981 *The Structure of Non-crystalline Materials Liquids and Amorphous Solids* (New York: McGraw-Hill)
[14] Wagner C N J and Ruppersberg H 1981 *At. Energy Rev.* **1** 101
[15] Fujiwara T 1989 *Phys. Rev.* B **40** 942